Global J. Environ. Sci. Manage. 7(2): 225-238, Spring 2021

Global Journal of Environmental Science and Management
(GJESM)

Homepage: https://www.gjesm.net/

ORIGINAL RESEARCH PAPER

# Two-dimensional flood model for risk exposure analysis of land use/land cover in a watershed

**G.R. Puno*, R.C.C. Puno, I.V. Maghuyop**

*College of Forestry and Environmental Science, Central Mindanao University, Musuan, Maramag, Philippines*

**ARTICLE INFO**

***Article History:***
Received 26 August 2020
Reviewed 16 September 2020
Revised 06 November 2020
Accepted 08 December 2020

***Keywords:***
Climate change
Hazards
Remote sensing
Resilience
Return period

**ABSTRACT**

**BACKGROUND AND OBJECTIVES:** The study involved developing a two-dimensional flood model to analyze the risk exposure of land use/land cover based on the generated flood hazard maps for the six return period scenarios in the Solana watershed.

**METHODS:** The approach consisted of applying hydrologic and hydraulic numerical flood models and the suite of advanced geographic information systems and remote sensing technologies. The process involved utilizing a high-resolution digital elevation model and a set of high-precision instruments such as the real-time kinematic-global position system receiver, digital flow meter, deep gauge, and automatic weather station in collecting the respective data on bathymetry, river discharge, river depth, and rainfall intensity during a particular climatic event, needed for the model development, calibration and validation.

**FINDINGS:** The developed two-dimensional flood model could simulate flood hazard with an 86% accuracy level based on the coefficient of determination statistics. The flood risk exposure analysis revealed that coconut is the most affected, with 31.3% and 37.1% being at risk across the 2-year and 100-year return period scenarios, respectively. Results also showed that rice and pineapple are at risk of flooding damage with the increasing rate of exposure by a magnitude of 42.9 and 9.3 across the 2-year and 100-year flood scenarios, respectively.

**CONCLUSION:** The study highlighted the integration of the findings and recommendations in the localized comprehensive land use plan and implementation to realize the challenge of building a climate change proof and a flood-resilient human settlement in the urbanizing watershed of Solana.

DOI: 10.22034/gjesm.2021.02.06

| NUMBER OF REFERENCES | NUMBER OF FIGURES | NUMBER OF TABLES |
|---|---|---|
| 43 | 9 | 3 |

*Corresponding Author:
Email: *grpuno@cmu.edu.ph*
Phone: +639166918259
Fax: +6388 356 1912

Note: Discussion period for this manuscript open until July 1, 2021 on GJESM website at the "Show Article.

## INTRODUCTION

Catastrophic floods following torrential rains brought by climate change-induced typhoons have recently recurred in the regions of Southeast Asian countries. The Philippines is one of the Southeast Asian countries recently hit by floods due to the three successive typhoons, namely Quinta, Rolly, and Ulysses, internationally known as Molave, Goni, and Vamco, respectively (De Vera-Ruiz, 2020; Teves, 2020). Disastrous floods brought about by these typhoons made the situation of the country worse amid coronavirus disease 2019 (COVID-19) pandemic. About millions of Filipinos moved to the evacuation facilities for safety, but their properties remained exposed to flood hazards and are at risk of devastation. Monitoring and assessing the affected areas for relief goods distribution and other possible mitigation purposes are the immediate disaster responses by the government and non-government organizations. In aid of legislation, academic institutions and research units may have to conduct a more detailed risk exposure analysis and assessment of the inundated sites using a standard set of statistical and flood modeling tools like the Hydrologic Engineering Center-Hydrologic Modeling System (HEC-HMS) and HEC-River Analysis System (Gumindoga *et al*., 2017; Khalfallah and Saidi, 2018). However, flood modeling for risk exposure analysis requires specific expertise and experience (The World Bank, 2016). The research team must have the basics in modeling, with background on the different climatic and hydrologic parameters, including the processes and the application of hydrologic and hydraulic models, geographic information systems (GIS), and remote sensing tools. The types of computer application software, equipment, and input data are also important factors that could affect the accuracy and validity of the final flood model (Ogania *et al*., 2019). Even with the availability of the above procedure, several flood modeling and simulation studies failed to elaborate the use of high precision real-time kinematic-global positioning system (RTK-GPS) equipment and high-resolution digital elevation model (DEM) data such as those derived from airborne light detection and ranging (LiDAR). The reason for this is the unavailability of high-resolution DEM data in some areas. For example, some flood modeling studies used low-resolution DEM such as those derived from Shuttle Radar Topography Mission and Synthetic Aperture Radar technologies (Zhang *et al*., 2019; Laks *et al*., 2017; Musa *at al*., 2015). The type of data, modeling protocols, and equipment used will eventually affect the reliability of results and the acceptability of the entire process of a GIS-based technique of flood risk exposure analysis and assessment. As reviewed, flood risk analysis and assessment is an emerging scientific discipline that emphasizes GIS, with some limitations, as the most promising tool having the capability to integrate all the other techniques (Diez-Herrero and Garrote, 2020). Appropriate flood modeling and hazard map generation techniques could enhance the risk exposure analysis and assessment study results, specifically with the use of high-resolution DEM and application of high precision surveying equipment, hydrologic and hydraulic models, and the combined technologies of GIS and remote sensing (Puno *et al*., 2019; Puno *et al*., 2018; Santillan *et al*., 2016). Nevertheless, regardless of methods limitations such as the unavailability of high-resolution LiDAR data and high-precision survey instrument like RTK, flood modeling, as an initial step, is essential to generate a hazard map for flood risk exposure and analysis of the inundated land use/land cover (LULC) within the watershed. Land use includes built-up areas, roads, bridges, buildings, and other infrastructures, while land cover comprises different types of vegetation like the forest, grasslands, agro-industrial, and other crop plantations (Israel and Briones, 2013). In the past few years, risk exposure and assessment projects in the Philippines enabled the generation of highly detailed flood hazard maps through LiDAR data (Sarmiento *et al*., 2015). The method allows the collection of high-resolution DEM data appropriate as input in the flood modeling simulation and hazard map generation using the hydrologic model and GIS technique. These programs/projects include the University of the Philippines Disaster Risk and Exposure Assessment for Mitigation (UP-DREAM) and its expansion, the Philippine Light Detection and Ranging 1, and the Geo-Informatics for the Systematic Assessment of Flood Effects and Risks for a Resilient Mindanao (Geo-SAFER Mindanao). On top of producing highly detailed flood hazard maps and updated high-resolution DEM covering two-thirds of the country's critical river basins and other priority areas, the above projects aimed at analyzing flood risk exposure of the affected LULC within the basins. The government and some non-government organizations have collaborated to conduct research programs deliberately to evaluate

the condition of LULC in the aftermath of flood hazards. The extent of damages to the affected LULC usually serves to account for the impact of the disaster on the local and national economies (Svetlana *et al*., 2015). Researchers worldwide have conducted flood risk exposure analysis and assessment studies to evaluate the vulnerability of LULC to flood hazards (Mousavi *et al*., 2019; Pant *et al*., 2016). As suggested from the previous study, the multi-criteria approach could improve the methods especially those involving decision-making relative to proper land-use zoning for flood mitigation (Motlagh and Sayadi, 2015). However, this study focuses only on developing a flood model as a basis for the risk exposure analysis of LULC in the Solana watershed. This paper presents the methods of developing, calibrating, and validating a two-dimensional (2D) flood model to analyze the risk exposure of LULC based on the hazard maps for the six return period scenarios. The procedures involved using hydrologic and hydraulic models such as HEC-HMS and HEC-RAS, respectively, within the GIS environment. The study covered the two municipalities of Claveria and Jasaan, Misamis Oriental, for one year in 2018-2019. This study expects the utilization of information on flood risk exposure analysis by the policy- and decision-making authorities in the quest of building an ecologically sustainable and flood-resilient community.

## MATERIALS AND METHOD

*The study watershed*

The study team selected the Solana watershed as the study site due to the periodic occurrence of fluvial flooding, causing inundation in the floodplain. Furthermore, the Environmental Management Bureau-Department of Environment and Natural Resources (EMB-DENR) prioritizes the river of Solana watershed to be under the water quality monitoring program of the government through its memorandum dated June 8, 2016. The area belongs to a tropical rainforest climate with an average daily temperature of 25°C. The rainfall is evenly distributed throughout the year with monthly average accumulations of 18.29 mm. The topography of the upper watershed is characterized by gently rolling hills and mountain ranges. The soil, particularly in Claveria is classified under Jasaan Clay with a deep of Ultic Haplorthox (Delgado and Canters, 2012). The Solana river under normal flow has an average of approximately 1.0 $m^3/s$ and peaks at 4.32 $m^3/s$ during an event. The watershed location is at the north-central of Misamis Oriental Province (Fig. 1). It lies between 124° 45' 46.02" to 124° 54' 45.33" east longitude and 8° 39' to 8° 35' north latitude, having a length of 17.60 km and a width of 3 km, and an estimated drainage area of 67.65 square kilometers. The watershed traverses the municipalities of Claveria and Jasaan of Misamis Oriental and drains into the Macajalar Bay.

*Data for flood modeling*

The process of flood risk exposure analysis consists of primary and secondary data collection and preparation. The collected sets of secondary data included the high-resolution DEM, soils, Sentinel 2 satellite image of land cover from the United States Geological Survey Earth Explorer, and the historical rainfall intensity duration frequency (RIDF). These

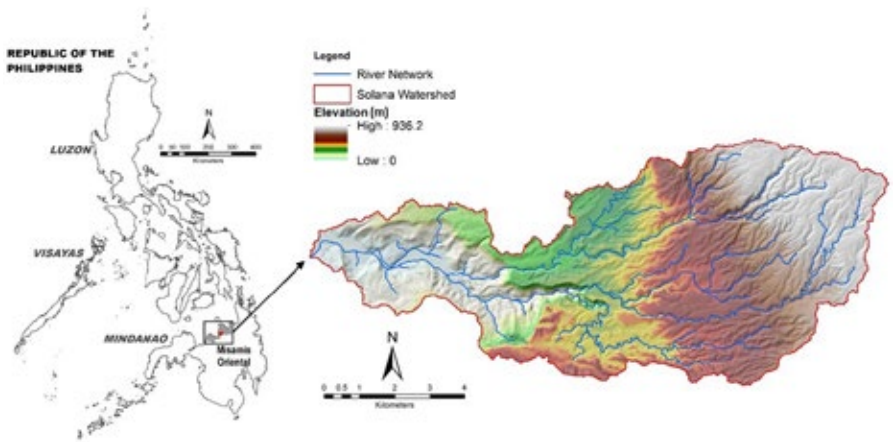



Fig. 1: Geographic location of Solana Watershed in north-central Misamis Oriental, Philippines

data were processed and prepared according to the set of procedures required in the modeling activity. The additional primary datasets included the rainfall intensity, river depth, and velocity during a particular event, bathymetric data, and the measurements of the river's cross-section and profile.

*DEM and soils map acquisition*

The DEM map layer consists of two categories, the 5-meter resolution interferometric synthetic aperture radar (IFSAR) and the 1-meter resolution derived from LiDAR technology. The National Mapping and Resource Information Authority (NAMRIA) had provided the IFSAR data for the hydrologic modeling of the watershed. In contrast, the UP DREAM program had made the LiDAR data available for the hydraulic modeling component. The Bureau of Soils and Water Management had provided the soil map with the corresponding database.

*LULC map generation and validation*

The study used the July 26, 2017, sentinel-2 satellite image product from the United States Geological Survey (USGS) Earth Explorer to generate the LULC map for the whole modeled watershed. The team chose the image because it was available being free from cloudiness and other obstruction. The Sentinel-2A is an advanced satellite image with a resolution applicable for various remote sensing applications (Nguyen *et al*., 2020; Puno, *et al*., 2019; Addabbo *et al.,* 2016). This step included pre-processing of satellite images to correct single-date sentinel-2A level-1C products from the effects of the top of atmosphere (TOA) reflectance. The product output was the sentinel-2A level-2A with the bottom of atmosphere (BOA) reflectance. TOA to BOA involved the use of a processor (Sen2Cor) running on the European Space Agency's (ESA) sentinel-2 toolbox using the sentinel application platform (SNAP) software (Warren *et al*., 2019). The level-2A output product includes the bands with three different resolutions (60m, 20m, and 10m). The 10-meter resolution bands, namely red, green, and blue (RGB) and near-infrared (NIR), were layer-stacked and exported in tag image file format (TIFF) as the final image utilized during the LULC classification. Also, the Green-red vegetation index (GRVI) and normalized difference vegetation index (NDVI) were derived from the sentinel-2 imagery to enhance further the LULC classification accuracy (Sothe *et al*., 2017; Zhang *et al*., 2017). This step performed an object-based image analysis using eCognition Developer version 9.0.1 to produce an output consisting of the grouping pixels as a segment rather than individual grids with combined spectral, spatial, and contextual information (Phiri and Morgenroth, 2017). The applied classification algorithm was the support vector machine (SVM), which provides better classification results and outperformed other classifiers such as the pixel-based maximum likelihood classifier (Ji *et al*., 2019; Bahari *et al*., 2014; Shi and Yang, 2015). SVM involves training sample collection from pixels of the image used to establish threshold as the basis of delineating specific land cover classes. The next phase consisted of collecting validation sample points of different land cover classes on the ground, independent from training samples collected based on the image of google earth aerial photos. The process involved applying the confusion matrix analysis using the training and validation sample points to obtain the producer, user, and the overall accuracy values (Janiola and Puno, 2018). The producer accuracy refers to the probability that a particular land cover class of an area on the ground is classified as such, while the user accuracy refers to the likelihood of the same identity between a pixel and the actual land cover class in the map (Rwanga and Ndambuki, 2017; Bogoliubova and Tymkow, 2014). The LULC classification output using eCognition produces several segmented objects as polygons where some are irrelevant in the map layout. Thus, the process applied the minimum mapping unit tool within the ArcGIS 10.2 to decongest the map from irrelevant segmented polygons. The process is necessary for the overall LULC classification to visually and spatially reduce the complexity of the information contained in the final map (Garcia-Alvarez *et al*., 2019).

*Event and bathymetric data collection*

The modeling team also collected data from a particular event like rainfall intensity, river depth, and velocity from the installed automatic weather station, digital depth gauge, and digital velocity meter, respectively. The study also obtained the RIDF from the Philippine Atmospheric, Geophysical, and Astronomical Services Administration (PAG-ASA). The team conducted the actual field survey of the channel cross-section and river reach using a high precision

RTK-GPS receiver instrument to collect bathymetric and river profile data.

*Flood model development, calibration, and validation*

The flood modeling component of this study involved two processes, that is, hydrologic and hydraulic model development. The modeling protocols applied the two open-source sets of computer utilities. The first set consists of the HEC-HMS responsible to simulate river discharge (Gumindoga *et al*., 2017). The second set comprises the HEC-River Analysis System version 5.0 (HEC-RAS 5.0) responsible to simulate a 2D flood model domain (Khalfallah and Saidi, 2018). Both models have the geospatial interface as an extension of ArcGIS 10.2 namely HEC-GeoHMS and HEC-GeoRAS. The HEC-GeoHMS enabled the team to delineate the watershed and the river network using the 5-m IFSAR DEM within the GIS environment. A total of 102 sub-watersheds were delineated within the main watershed. The team then proceeded with the series of flood simulation runs and generating of hydrograph based on the land cover map from Sentinel 2, soils map, and the localized rainfall and river velocity data from June 5-6, 2018 event. HEC-HMS and HEC-RAS are a suite of computer models consisting of several equations, thus, the presentation of such in this report is unnecessary (Castro and Maidment, 2020). The modeler did the calibration to fit the simulated and observed hydrographs by adjusting the model parameters (Sarchani and Tsanis, 2019; Wang *et al*., 2018). These parameters include the recession constant, ratio-to-peak, and Manning's n-values with the adjusted values of 0.4, 0.3, and 0.05, respectively, set as the final inputs for the main watershed. The other parameter number is specific to 102 sub-watersheds. Therefore, the average values of 78.81, 25.23, 1.44, 1.84, and 0.0125 for the curve number, initial abstraction, storage coefficient, time of concentration, and the initial base flow, respectively, are presented for the main watershed. Finally, the research team had evaluated the model performance by comparing the simulated and observed values using the coefficient of determination ($R^2$), Nash-Sutcliffe efficiency (NSE), root mean square errors-observations standard deviation ratio (RSR), and percent bias (PBIAS) statistics (Melaku *et al*., 2020). The calibrated flood model was the input in the hydraulic modeling phase to produce the 2D model domain map for the Solana watershed. The activity flowed the details of the 2D model development employed from the previous study's procedures (Santillan *et al*., 2016). This involves utilizing a delineated 2D flow area that represents the floodplain of the Solana river (Fig. 2). The 2D flow area consists of boundary conditions, namely the flow hydrographs indicating the inflows where discharge from the upstream starts to flow, the stage hydrograph at the river outlet considering the tidal boundary condition data in the Macalajar Bay, and the precipitation boundary condition. The delineated break lines across the river were also added indicating the abrupt changes in elevation such as the riverbanks and roads. The LiDAR DEM incorporated with actual riverbed information using bathymetric burning from field survey was the model simulation's primary input file. Using the bathymetric burned DEM, the simulated discharge will flow considering the river bed's elevation, improving the water volume estimations along river and floodplains of the watershed (Siev *et al*., 2016). Also, Manning's roughness coefficient values of specific land cover had influenced the simulated flood extent and depth of the hydraulic model.

The team validated the accuracy performance of the Solana 2D hydraulic model through ground cross-examination using field data associated with the simulated flood according to a particular historic rainfall event. A field validation survey was conducted through individual interviews from the locals, either flooded or not flooded, using predetermined random points within the floodplain.

*Flood hazard map generation*

The values of the calibrated and validated hydrograph developed in the hydrologic modeling component were then used as an input in the hydraulic modeling phase to generate a hazard map detailing the extent and depth of flood for the six return periods corresponding to 2-year, 5-year, 10-year, 25-year, 50-year, and 100-year scenarios. The simulation of the six return period flood scenarios was based on the long historical rainfall intensity duration frequency (RIDF) obtained from the Philippine Atmospheric, Geophysical, and Astronomical Services Administration (PAGASA). The final flood hazard index map consists of three categories according to flood depth such as low (<0.50m), medium (0.50m to 1.50m), and high (>1.50m).

*Feature extraction and flood exposure analysis*

The extraction procedure used the digital surface

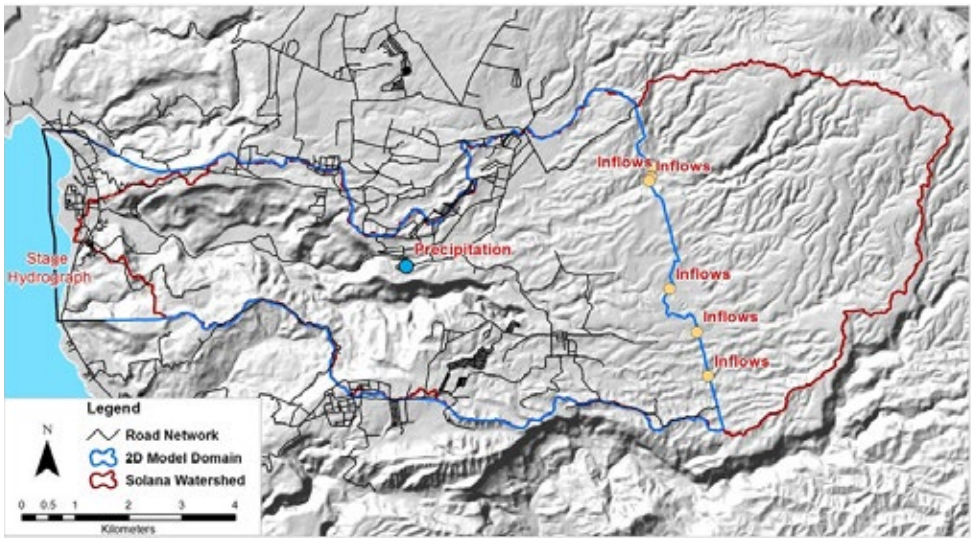



Fig. 2: Boundary conditions in the 2D model domain in Solana watershed.

model (DSM) component of LiDAR DEM data to manually extract the LULC features within the flooded surface. DSM is a type of elevation data that specifies LULC and other artificial features on the ground. High-resolution satellite images from Google Earth and Google Street View from the internet were also utilized as additional map layers in the feature extraction process, particularly in areas not covered by DSM. Validation of manually extracted features was done through geotagging activity of the identified and attributed LULC. The attributed LULC map was then used for the final risk exposure analysis of the 2D flood model domain of the watershed. Finally, the flood exposure analysis was through the cross-tabulation method of the exposed LULC according to the six return period flood scenarios.

## RESULTS AND DISCUSSION

*Land use/land cover map*

The LULC map (Fig. 3) map of the Solana watershed generated using an object-based SVM algorithm obtained a higher accuracy based on the training sample points and validation sample points from the ground. The evaluation was made through confusion matrix analysis using the two sets of sample coordinate points from the ground validation survey and the satellite image, respectively (Xu *et al*., 2020). The confusion matrix analysis for the predicted and observed LULC classes revealed the producer accuracy values of 95, 83, 82, 89, 89, 100, 70, 100, 72, 93, 70, 100, 70 percent and the user accuracy values of 83, 94, 83, 96, 99, 100, 95, 100, 70, 93, 100, 71, and 100 percent for the open/cultivated, isolated trees, coconut, pineapple, buildings, banana, mango, water, tree plantation, road, shrubland, rice, and grassland, respectively. The analysis obtained an 88.05% overall accuracy. Table 1 shows the details of the land cover distribution by area. The flooded infrastructures, namely building and road comprise about 1.59% and 0.46%, respectively. As shown, open/cultivated land is the dominant land cover of the area, suggesting that more than half of the watershed is agriculturally active for crop production. Open/cultivated soil indicates that the Solana watershed is prone to flooding as the surface runoff accumulates quickly and flushes into the rivers and floodplains due to the removal of the protective forest cover (Bhattacharjee and Behera, 2018).

*Calibrated and validated flood model*

Flow routing and flood modeling for the watershed utilized the discharge time-series data from June 5 to 6, 2018, with a peak of 4.32 $m^3/s$ (Fig. 4). The total precipitation relative to the observed peak discharge was 36.2 mm, with a maximum of 10.2 mm per 10-minute interval. These values served as inputs in calibrating the hydrologic model of the Solana watershed. Fitting the observed and simulated

Table 1: LULC distribution in the watershed

| LULC | Area (ha) | % of the Total |
|---|---|---|
| Open/cultivated | 4153.06 | 61.38 |
| Isolated trees | 1058.93 | 15.65 |
| Coconut | 948.61 | 14.02 |
| Pineapple | 257.37 | 3.80 |
| Building | 107.46 | 1.59 |
| Banana | 50.32 | 0.74 |
| Mango | 42.19 | 0.62 |
| Water | 35.63 | 0.53 |
| Tree Plantation | 32.33 | 0.48 |
| Road | 30.89 | 0.46 |
| Shrubland | 26.94 | 0.40 |
| Rice | 15.06 | 0.22 |
| Grassland | 7.58 | 0.11 |
| Total | 6,766.37 | 100.00 |

discharge values yielded a satisfactory result with a coefficient correlation of 86% (Fig. 5). The overall model calibration performance obtained a very good statistical agreement between the simulated and observed values with NSE, RSR, and PBIAS of 0.75, 0.50, and -5.77, respectively, implying acceptable model results. These findings indicate that the simulated flood behavior is as good as the observed flood from an actual event. Moreover, the model could generate different flood events using any rainfall scenario with an 86% accuracy level. Thus, the model is technically acceptable to generate flood hazard index maps at six different return period scenarios from any hypothetical and real rainfall events.

The historical rainfall event of tropical storm Sendong, internationally known as Washi in 2011 was the benchmark for the validation survey in coordination with the localities within the Solana watershed. However, due to the unavailability of Sendong rainfall data from the Solana watershed, the process interpolated the historical data from six PAGASA stations, namely Butuan, Lumbia, Malaybalay, Cotabato, General Santos, and Davao weather stations containing the rainfall record of Sendong for the flood model simulation and evaluation. Fig. 6 shows the simulated flood depth and flood extent based on the Sendong event at the Solana watershed. Flood extent covered the north of the 2D model domain outside the Solana watershed which is approximately 700 meters away from the main Solana river. This observation implies that some communities were still affected by floods during torrential rains even when they are at a certain distance away from the river.

*Flood hazard map for the six return periods*

Fig. 7 shows the 6-return period scenarios flood hazard maps from the calibrated and validated HEC-RAS model. The 2-year, 5-year, 10-year, 25-year, 50-year, and 100-year return periods of flood events would mean a 50%, 20%, 10%, 4%, 2%, and 1% likelihood of recurrence within a year, respectively (Apollonio *et al.*, 2020). The basis of choosing the six return period scenarios was the recurrence of floods in the area, which is almost every year. The number

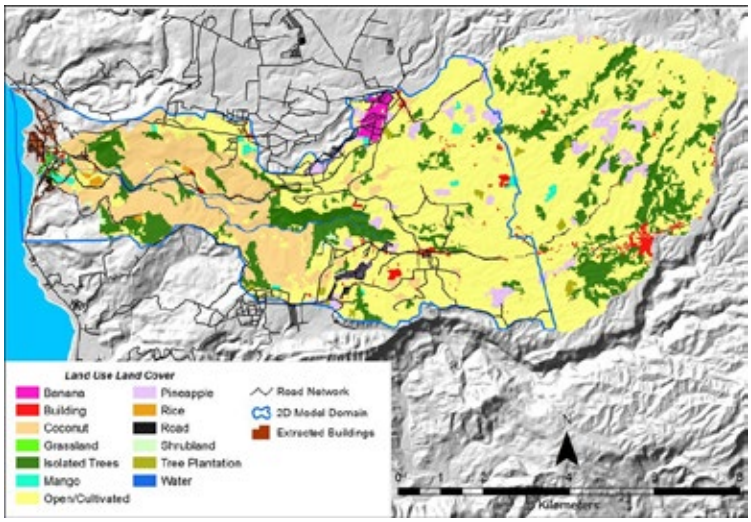



Fig. 3: Land use land cover map of Solana watershed

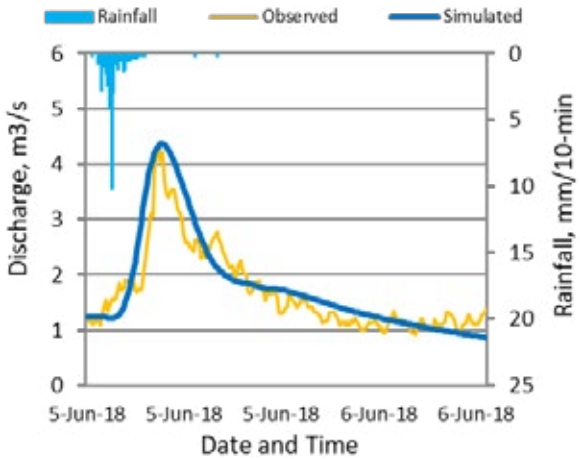



Fig. 4: Hydrograph for observed and simulated discharge data

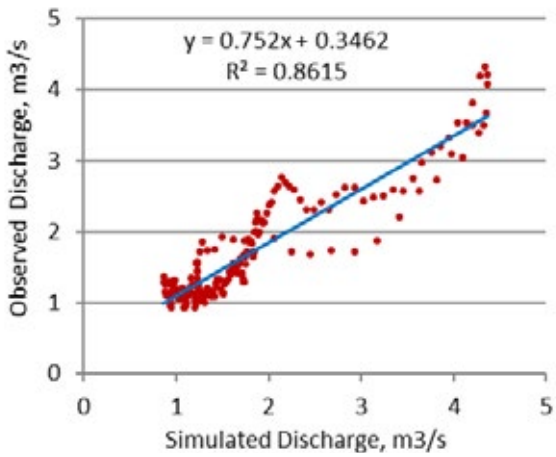



Fig. 5: Correlation between observed and simulated discharge data

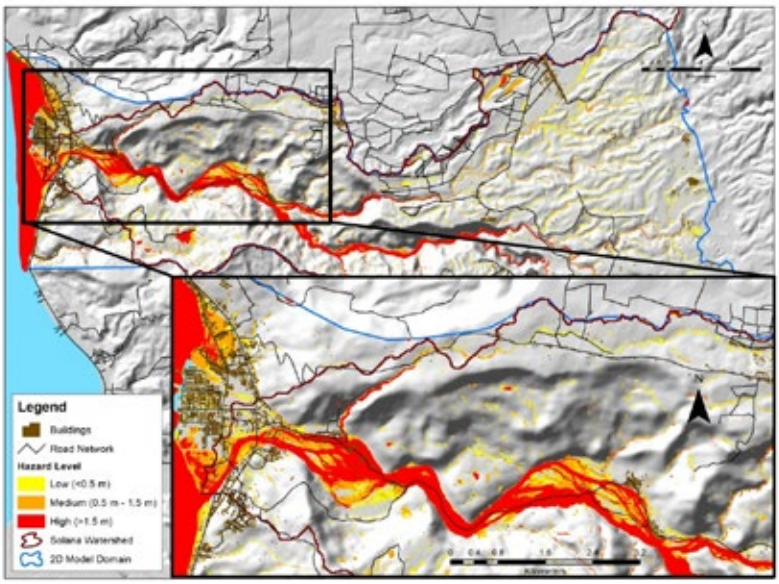



Fig. 6: Flood hazard map of 2011 tropical storm Sendong in Solana watershed

of years in the scenario was chosen arbitrarily. The generated flood hazard maps for the six return period scenarios conformed with the other studies showing the apparent increases of flooded areas with the delay of the return period (Shrestha and Lohpaisankrit, 2017). Fig. 7 depicts that the areas susceptible to flooding are mostly near the river, extending towards the floodplain of the watershed. These areas have the most affected households because of the increasing population. Additionally, the infrastructures that critically define the growing local economy are within these areas. Thus, the study site is highly vulnerable to flood hazards. This study underscores that flood modeling and hazard map generation is a helpful initiative for flood risk exposure analysis. Results of such analysis are vital in reducing and mitigating the impact of flood hazards in an urbanizing Solana watershed (Sharif *et al*., 2016).

*Flood exposure analysis*

The analysis yielded a total of 5,467 extracted buildings within the 2D model domain of the Solana

watershed, with the risk exposure of 22.0% to low, medium, and high levels of flood hazards during the 2-year return period scenario. This percentage of exposed land use or buildings had continuously increased with the succeeding chances of flood recurrence, maximizing 56.1% during the 100-year return period scenario (Fig. 8). This finding would mean that 78% of the buildings were initially not exposed to flood hazards during the 2-year return period. However, this percentage was reduced to 43.9%, implying that the exposure of the building to flood hazards would increase by more than half during the 100-year return period scenario. For the low level (<0.5m depth) flood risk, about 11.6% of the buildings were exposed during the 2-year return period and increased to 16.4% during the 100-year return period. Increases of the exposed structures for the compared scenarios were also evident for

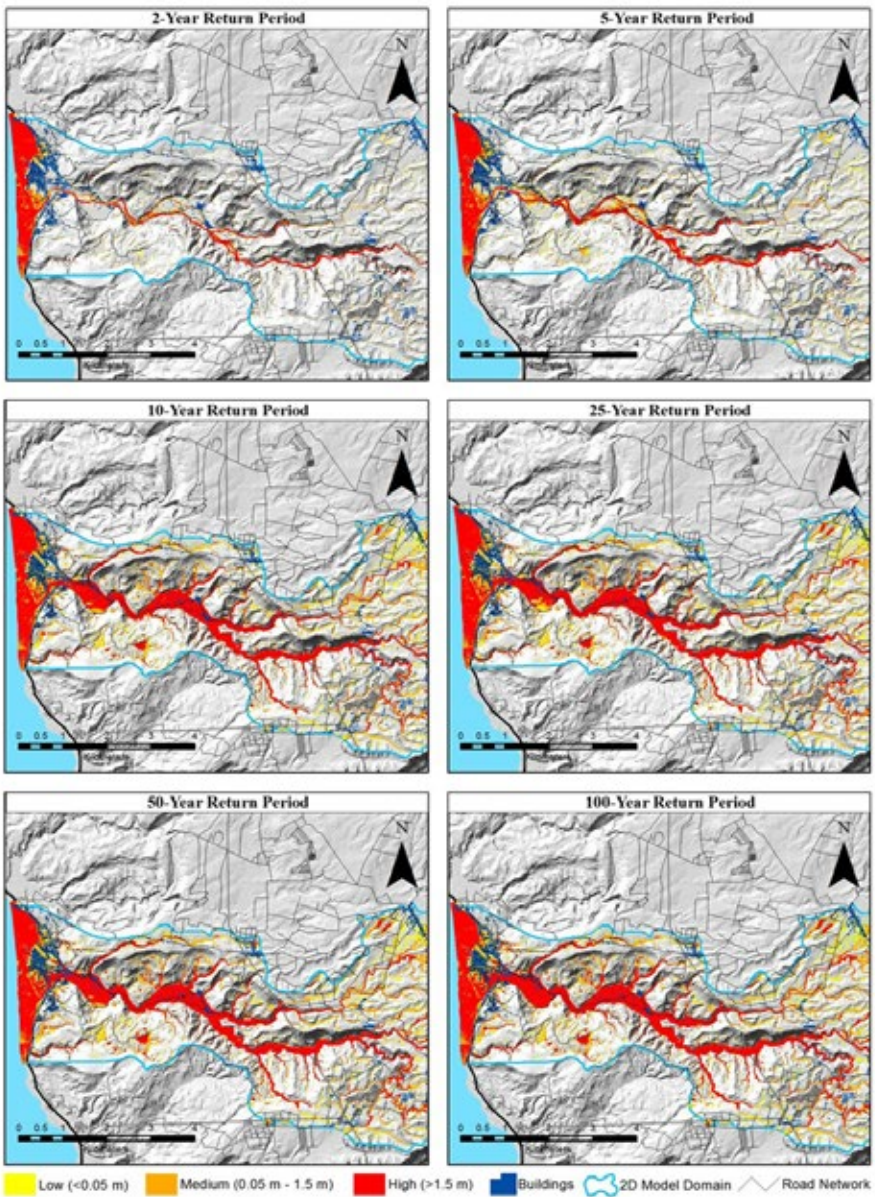
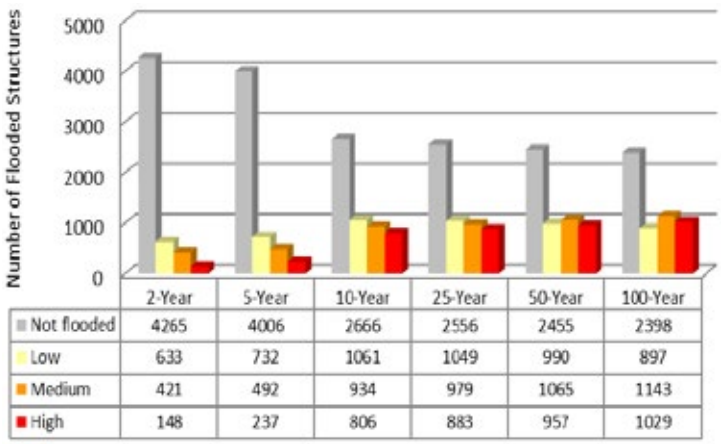



Fig. 7: Flood hazard maps in Solana watershed for the six return period scenarios.

both the medium (0.5m-1.5m) and high (>1.5m) flood levels. The cross-tabulation analysis shows an increasing pattern of exposed buildings as the return period covers a longer duration, and as the level of flood hazard reduces. However, some discrepancies of the pattern were obvious such as the cases of 50-year and 100-year return periods where the number of exposed structures had increased from low to medium risk level (Fig. 8). A similar increasing pattern and discrepancies of flood risk exposure of infrastructure across the return period were also revealed from previous studies (Apollonio *et al.*, 2020).

Fig. 9 shows the different land cover, including the road being exposed to flooded risk under the 1.50m depth for the six return period scenarios within the 2D flood model domain. The most extensive affected land cover was coconut, which is consistently higher in the six return period scenarios because it covers almost the watershed floodplain. Tree plantation, mango, and banana are the least exposed as they are usually occupying high-elevated sites. Table 2 presents a summary of the inundated land cover for the six return period scenarios. Cross-tabulation analysis of results shows an increasing pattern of percent risk exposure based on the total by return period scenarios (Table 3). The increase of flood risk exposure of various LULC is also reported from previous researches for 25-year, 50-year, and 100-year floods recurrences (Shrestha and Lohpaisankrit,




| | 2-Year | 5-Year | 10-Year | 25-Year | 50-Year | 100-Year |
|---|---|---|---|---|---|---|
| Not flooded | 4265 | 4006 | 2666 | 2556 | 2455 | 2398 |
| Low | 633 | 732 | 1061 | 1049 | 990 | 897 |
| Medium | 421 | 492 | 934 | 979 | 1065 | 1143 |
| High | 148 | 237 | 806 | 883 | 957 | 1029 |

Fig. 8: Flooded structures in Solana watershed for the six flood scenarios at different hazard levels

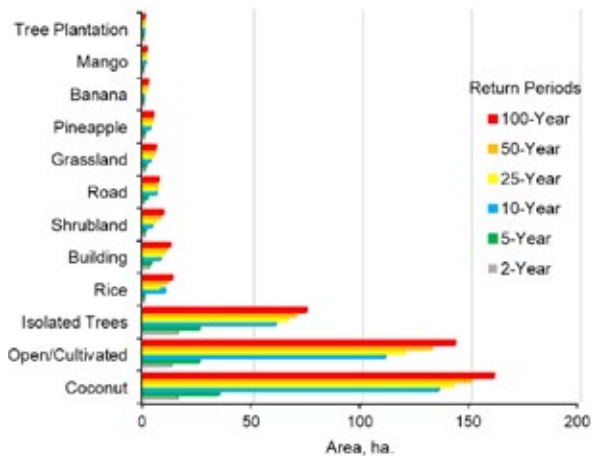



Fig. 9: Land use/land cover in Solana watershed exposed to flood hazard

Table 2: Percentage (%) of flood risk exposure by total across land cover

| Land Cover | Return period scenarios | | | | | |
|---|---|---|---|---|---|---|
| | 2-Year | 5-Year | 10-Year | 25-Year | 50-Year | 100-Year |
| Coconut | 31.3 | 36.6 | 39.6 | 38.7 | 37.5 | 37.1 |
| Open/Cultivated | 25.8 | 27.0 | 32.4 | 32.6 | 33.0 | 33.0 |
| Isolated Trees | 31.7 | 27.1 | 17.7 | 18.0 | 17.5 | 17.2 |
| Rice | 0.6 | 0.5 | 2.9 | 2.1 | 2.7 | 3.0 |
| Building | 5.5 | 3.7 | 2.3 | 2.5 | 2.7 | 2.8 |
| Shrubland | 1.7 | 1.0 | 1.1 | 1.5 | 1.9 | 2.1 |
| Road | 0.5 | 1.9 | 1.7 | 1.7 | 1.6 | 1.6 |
| Grassland | 1.9 | 1.3 | 0.9 | 1.2 | 1.3 | 1.3 |
| Pineapple | 0.9 | 0.8 | 0.9 | 1.0 | 1.0 | 1.0 |
| Banana | 0.0 | 0.0 | 0.0 | 0.3 | 0.4 | 0.5 |
| Mango | 0.0 | 0.0 | 0.2 | 0.3 | 0.2 | 0.3 |
| Tree Plantation | 0.0 | 0.0 | 0.1 | 0.1 | 0.1 | 0.1 |

Table 3: Percentage (%) of flood risk exposure by total across return periods

| LULC | Return period scenarios | | | | | |
|---|---|---|---|---|---|---|
| | 2-Year | 5-Year | 10-Year | 25-Year | 50-Year | 100-Year |
| Coconut | 2.5 | 5.4 | 21.2 | 22.2 | 23.5 | 25.2 |
| Open/Cultivated | 2.4 | 4.7 | 20.4 | 22.0 | 24.3 | 26.3 |
| Isolated Trees | 5.1 | 8.2 | 19.3 | 21.1 | 22.4 | 23.9 |
| Rice | 0.7 | 1.1 | 23.1 | 18.4 | 25.6 | 31.1 |
| Building | 6.0 | 7.7 | 17.0 | 19.7 | 23.1 | 26.4 |
| Shrubland | 3.0 | 3.5 | 14.0 | 19.4 | 27.8 | 32.2 |
| Road | 1.0 | 6.5 | 21.6 | 22.7 | 23.1 | 25.1 |
| Grassland | 4.7 | 6.1 | 15.5 | 20.6 | 25.7 | 27.5 |
| Pineapple | 2.8 | 4.8 | 18.9 | 22.1 | 25.1 | 26.3 |
| Banana | 0.0 | 0.0 | 0.6 | 24.2 | 34.3 | 40.9 |
| Mango | 0.2 | 0.2 | 20.3 | 23.1 | 23.0 | 33.3 |
| Tree Plantation | 0.2 | 0.4 | 19.8 | 24.6 | 26.2 | 28.9 |

2017). This result suggests that the longer the return period, the more hazardous the flooding scenario is.

Among the identified economically significant land cover in the area include rice and pineapple. Cross-tabulation analysis of results shows that the flood risk exposure of rice in percent for the six return period scenarios starting from the 2-year flood, had increased by a magnitude of 1.5, 31.9, 25.5, 35.3, and 42.9 for the 5-, 10-, 25-, 50-, and 100-year flood scenarios, respectively. Similarly, the flood risk exposure of pineapple had increased by a magnitude of 1.7, 7.7, 7.8, 8.9, and 9.3 for the considered flood scenarios, respectively. Unlike other perennial crops such as trees, coconut, and mango, rice and pineapple are vulnerable to damage when frequently exposed to flood hazards for a longer duration. Hence, decision-makers must prioritize these crops in terms of proper LULC planning and zoning to mitigate the negative impact of flood hazards on crop production in the future. The results also suggest identifying appropriate sites for built-ups and climate change-proof road designs to minimized flood exposure of these key features of the local and national economy.

## CONCLUSION

The study enabled the application of HEC-HMS and HEC-RAS with the integration of advanced GIS and remote sensing technologies to develop a 2D flood model for risk exposure analysis and assessment of LULC within the Solana watershed. Emphasized in the study was the use of high precision RTK-GPS and high-resolution LiDAR-derived DEM. The method also included the use of a digital instrument such as a river velocity meter, deep gauge, and rain gauge through AWS in the gathering of rainfall and river discharge data for model development, calibration, validation, and evaluation. The study generated the flood hazard maps for the six return period scenarios. The research

team successfully calibrated the model with an 86% correlation between the observed and simulated discharge. The model input LUCL map of the watershed generated from the sentinel-2 satellite images with an accuracy level of 88.05% based on the confusion matrix analysis, showed that the open/cultivated land is the dominant land cover with 61.38% of the total area indicating high susceptibility to flooding. The study successfully analyzed the flood exposure of the various LULC of the site based on the generated flood hazard maps for the six return period scenarios. The result of exposure analysis showed that coconut plantation was the most affected LULC having 31.3% and 37.1% across the 2-year and 100-year return period scenarios, respectively. The least affected land covers were timber and fruit tree plantation because they are generally at higher elevations. Results also showed the increasing exposure of rice fields and pineapple plantations to flood hazards by a magnitude of 42.9 and 9.3 across the 2-year and 100-year scenarios, respectively. These crops have high economic potential, but highly vulnerable to flood damage when exposed to flood hazards for a longer duration. Thus, local and national authorities need to prioritize these crops in terms of appropriate LULC zoning and planning to minimize the negative economic impact of flood hazards. The model also produced maps that capture a densely populated settlement within the floodplain of the watershed, indicating high-risk exposure and vulnerability of such communities to flood hazards. This study emphasizes the identification of appropriate sites for built-ups and the development of climate change proof road designs based on the findings. Furthermore, the decision-makers must identify the strategic location of the evacuation center with safe access roads as recommended for more effective flood risk management within the urbanizing study watershed. This study also anticipates that the policy-making authorities must take advantage of the information in the challenge of creating a flood-resilient human settlement.

## AUTHOR CONTRIBUTIONS

G.R. Puno spearheaded the research project, wrote the manuscript, prepared the GIS databases, thematic map layers, layout design, and graphs. R.C.C. Puno generated the land cover map using satellite images, performed the flood modeling activities, and edited the manuscript. I.V. Maghuyop did the logistics of the project operation and edited the manuscript.

## ACKNOWLEDGMENTS

This paper is a product of the "Geo-Informatics for the Systematic Assessment of Flood Effects and Risks in Northern Mindanao and Cotabato, Philippines (Geo-SAFER Northern Mindanao/Cotabato) Project No. 2, funded by the [DOST-PCIEERD: Acct.1: 416-154]. The authors also thank the Central Mindanao University administration and the local government units of Jasaan, Misamis Oriental for the support in the implementation and completion of the project.

## CONFLICT OF INTEREST

The authors declare no potential conflict of interest regarding the publication of this work. Besides, the ethical issues including plagiarism, informed consent, misconduct, data fabrication and, or falsification, double publication and, or submission, and redundancy have been completely witnessed by the authors.

## ABBREVIATIONS

| | |
|---|---|
| *2D* | Two-Dimensional |
| *BOA* | Bottom of atmosphere |
| *DEM* | Digital elevation model |
| *DSM* | Digital surface model |
| *PCIEERD-DOST* | Philippine Council for Industry, Energy and Emerging Technology Research and Development-Department of Science and Technology |
| *EMB-DENR* | Environmental Management Bureau-Department of Environment and Natural Resources |
| *ESA* | European Space Agency |
| *Geo* | Geospatial |
| *Geo-SAFER-Mindanao* | Geo-Informatics for the Systematic Assessment of Flood Effects and Risks for a Resilient Mindanao |
| *GIS* | Geographic information system |
| *ha* | Hectare |
| *GRVI* | Green-red vegetation index |
| *HEC-HMS* | Hydrologic Engineering Center-Hydrologic Modeling System |
| *HEC-RAS* | Hydrologic Engineering Center-River Analysis System |
| *ISAR* | Interferometric synthetic aperture radar |
| *km* | kilometer |

| | |
|---|---|
| *LiDAR* | Light detection and ranging |
| *LULC* | Land use/land cover |
| *m* | Meter |
| *mm* | Millimeter |
| *NAMRIA* | National Mapping and Resource Information Authority |
| *NDVI* | Normalized difference vegetation index |
| *NIR* | Near-infra red |
| *NSE* | Nash-Sutcliffe efficiency |
| *PAGASA* | Philippine Atmospheric, Geophysical, and Astronomical Services Administration |
| *PBIAS* | Percent bias |
| $R^2$ | Coefficient of determination |
| *RGB* | Red, green, and blue |
| *RIDF* | Rainfall intensity duration frequency |
| *RSR* | Root mean square errors-observations standard deviation ratio |
| *RTK-GPS* | Real-time kinematic-global positioning system |
| *SNAP* | sentinel application platform |
| *SVM* | Support vector machine |
| *TIFF* | Tag image file format |
| *TOA* | Top of atmosphere |
| *UP DREAM* | University of the Philippines Disaster Risk and Exposure Assessment for Mitigation |

## REFERENCES


Addabbo, P.; Focareta, M.; Marcuccio, S.; Votto, C.; Ullo, S. L., (2016). Contribution of sentinel-2 data for applications in vegetation monitoring. Acta Imeko, 5(2): 44–54 (**11 pages**).

Apollonio, C.; Bruno, F.M.; Iemmolo, G.; Molfetta, M.G.; Pellicani, R., (2020). Flood risk evaluation in ungauged coastal areas: The case study of Ippocampo (Southern Italy). Water, 2020(12): (**25 pages**).

Bahari, N.I.S; Ahmad, A.; Aboobaider, B.M., (2014). Application of support vector machine for classification of multispectral data. IOP Conf. Ser.: Earth Environ. Sci., 20(2014): 1-8 (**8 pages**).

Bhattacharjee, K.; Behera, B., (2018). Does forest cover help prevent flood damage? Empirical evidence from India. Global Environ. Change, 53: 78-89 (**12 pages**).

Bogoliubova, A.; Tymkow, P., (2014). Accuracy assessment of automatic image processing for land cover classification of St. Petersburg protected area. Acta Sci. Pol. Geod. Descr. Terr., 13 (1-2): 5-22 (**18 pages**).

Castro, C.; Maidment, C.V., (2020). GIS preprocessing for rapid initialization of HEC-HMS hydrological basin models using web-based data services. Environ. Modell. Software, 130: 104732 (**12 pages**).

Delgado, M.E.M.; Canters, F., (2012). Modeling the impacts of agroforestry systems on the spatial patterns of soil erosion risk in three catchments of Claveria, the Philippines. Agrofor. Syst., 85: 411-423 (**13 pages**).

De Vera-Ruiz, E., (2020). Typhoon 'Rolly' may be as strong as 185 kph; may trigger signal No. 3 or 4 – PAGASA. Manila Bulletin.

Diez-Herrero, A.; Garrote, J., (2020). Flood risk analysis and assessment, applications and uncertainties: a bibliometric review. Water, 12(2050): 1-24 (**24 pages**).

Garcia-Alvarez, D.; Olmedo, M.T.C.; Paegelow, M., (2019). Sensitivity of a common Land Use Cover Change (LUCC) model to the Minimum Mapping Unit (MMU) and Minimum Mapping Width (MMW) of input maps. Compt. Environ. Urban Syst., 78: 101389 (**14 pages**).

Gumindoga, W.; Rwasoka, D.T.; Nhapi, I.; Dube, T., (2017). Ungauged runoff simulation in Upper Manyame Catchment, Zimbabwe: Application of the HEC-HMS model. Phys. Chem. Earth., 100: 371-382 (**12 pages**).

Israel, D.C.; Briones, R.M., (2013). Impacts of natural disasters on agriculture, food security, and natural and environment in the Philippines. ERIA Discussion Paper Series, (**54 pages**).

Janiola, M.D.C.; Puno, G.R., (2018). Land use and land cover (LULC) change detection using multitemporal landsat imagery: A case study in Allah Valley Landscape in Southern, Philippines. J. Biodivers. Environ. Sci., 12(2): 98-108 (**11 pages**).

Ji, Y.; Sun, L.; Li, Y.; Li, J.; Liu, S.; Xie, X.; Xu, Y., (2019). Non-destructive classification of defective potatoes based on hyperspectral imaging and support vector machine. Infrared Phys. Technol., 99: 71-79 (**9 pages**).

Khalfallah, B.C.; Saidi, S., (2018). Spatiotemporal floodplain mapping and prediction using HEC-RAS - GIS tools: Case of the Mejerda river, Tunisia. J. Afr. Earth. Sci., 142: 44-51 (**8 pages**).

Laks, I.; Sojka, M.; Walczak, Z.; Wrozynski, R., (2017). Possibilities of Using Low Quality Digital Elevation Models of Floodplains in Hydraulic Numerical Models. Water. 9(4): 1-19 (**19 pages**).

Melaku, N.D.; Wang, J.; Meshesha, T.W., (2020). Improving hydrologic model to predict the effect of snowpack and soil temperature on carbon dioxide emission in the cold region peatlands. J. Hydrol., 587: 124939 (**11 pages**).

Motlagh, Z.K.; Sayadi, M.K., (2015). Siting MSW landfills using MCE methodology in GIS environment. Case study: Birjand plain, Iran. Waste Manage., 46: 322-337 (**16 pages**).

Mousavi, S.D.; Roostaei, S.; Rostamzadeh, H., (2019). Estimation of flood land use/land cover mapping by regional modeling of flood hazard at sub-basin level case study: Marand basin. Geomatics, Natural Hazards and Risk. Geomatics Nat. Hazards Risk. 10(1): 1155-1175 (**21 pages**).

Musa, Z.N.; Popescu, I.; Mynett, A., (2015). A review of applications of satellite SAR, optical, altimetry and DEM data for surface water modelling, mapping and parameter estimation. Hydrol. Earth Syst. Sci., (19)9: 3755–3769 (**15 pages**).

Nguyen, H.T.T.; Doan, T.M.; Tomppo, E.; McRoberts, R., (2020). Land use/land cover mapping using multitemporal Sentinel-2 imagery and four classification methods - A case study from Dak Nong, Vietnam. Remote Sens., 12(9): 1367 (**27 pages**).

Ogania, J.L.; Puno, G.R.; Alivio, M.B.T.; Taylaran, J.M.G., (2019). Effect of digital elevation model's resolution in producing flood hazard maps. Global J. Environ. Sci. Manage., 5(1): 95-106 (12 pages).

Pant, R.; Thacker, S.; Hall, J.W.; Alderson, D.; Barr, S., (2016). Critical infrastructure impact assessment due to flood exposure. J. Flood Risk Manage., 11(1) (**20 pages**).

Phiri, D.; Morgenroth, J., (2017). Developments in Landsat land cover classification methods: A review. Remote Sens. 9(9): 1-25 (**25 pages**).

Puno, R.C.C.; Puno, G.R.; Talisay, B.A.M., (2019). Hydrologic responses of watershed assessment to land cover and climate change using soil and water assessment tool model. Global J. Environ. Sci. Manage., 5(1): 71-82 (**12 pages**).

Puno, G.R.; Amper, R.A.L.; Opiso, E.M.; Cipriano, J.A.B., (2019). Mapping and analysis of flood scenarios using numerical models and GIS techniques. Spat. Inf. Res., 28: 215-226 (**12 pages**).

Puno, G.R.; Amper, R.A.L.; Talisay, B.A.M., (2018). Flood simulation using geospatial and hydrologic models in Manupali Watershed, Bukidnon, Philippines. J. Biodivers. Environ. Sci., 12(3): 294-303 **(10 pages).**

Rwanga, S.; Ndambuki, J.M., (2017). Accuracy assessment of land use/land cover classification using remote sensing and GIS. Int. J. Geosci. 8. 611-622 (**12 pages**).

Santillan, J.R.; Marqueso, J.T.; Makinano-Santillan, M.; Serviano, J.L., (2016). Beyond flood hazard maps: detailed flood characterization with remote sensing, GIS and 2d modeling. In: Int. Arch. Photogramm. Remote Sens. Spatial Inf. Sci., XLII-4/W1, 225-235 (**11 pages**).

Sarchani, S.; Tsanis, I., (2019). Analysis of a flash flood in a small basin in Crete. Water, 11(11): 2253 (**22 pages**).

Sarmiento, C.J.; Ang, M.R.C.; Paringit E.C., (2015). LiDAR data acquisition and processing for Cagayan de Oro-Iponan river floodplains, disaster risk and exposure for mitigation (DREAM), DOST grants-in-aid program report, **(57 pages).**

Sharif, H.O.; Al-Juaidi, F.H.; Al-Othman, A.; Al-Dousary, I.; Fadda, E.; Jamla-Uddeen, S.; Elhassan, A., (2016). Flood hazards in an urbanizing watershed in Riyadh, Saudi Arabia. Geomatics Nat. Hazards Risk, 7(2): 702-720 (**19 pages**).

Shi, D.; Yang, X., (2015). Support Vector Machines for Land Cover Mapping from Remote Sensor Imagery. Monitoring and Modeling of Global Changes: A Geomatics Perspective. Springer Remote Sens./Photogrammetry. 265-279 (**15 pages**).

Shrestha, S.; Lohpaisankrit, W., (2017). Flood hazard assessment under climate change scenarios in the Yang River Basin, Thailand. Int. J. Sustainable Built Environ., 6(2): 285-298 (**14 pages**).

Siev, S.; Paringit, E.C.; Yoshimura, C.; Hul, S., (2016). Seasonal changes in the inundation area and water volume of the Tonle Sap River and its floodplain. Hydrol., 3(33): 1-12 (**12 pages**).

Sothe, C.; de Almeida, C.M.; Liesenberg, V.; Schimalski, M.B., (2017). Evaluating Sentinel-2 and Landsat-8 data to map successional forest stages in a subtropical forest in Southern Brazil. Remote Sens., 9(838): 1-22 (**22 pages**).

Svetlana, D.; Radovan, D.; Jan, D., (2015). The economic impact of floods and their importance in different regions of the world with emphasis on Europe. Procedia, 34: 649-655 (**7 pages**).

Teves, C., (2020). 3 Luzon dams brace for 'Ulysses'. Philippine News Agency.

The World Bank, (2016). Methods in flood hazards and risk assessment. Technical Notes, (**28 pages**).

Warren, M.A.; Simis, S.G.H.; Martinez-Vincente, V.; Poser, K.; Bresciani, M.; Alikas, K.; Spyrakos, E.; Giardino, C.; Ansper, A., (2019). Assessment of atmospheric correction algorithms for the Sentinel-2A MultiSpectral Imager over coastal and inland waters. Remote Sens. Environ., 225: 267-289 (**23 pages**).

Xu, J.; Zhang, Y.; Miao, D., (2020). Three-way confusion matrix for classification: A measure driven view. Inf. Sci., 507: 772-794 (**23 pages**).

Zang, T.; Su, J.; Liu, C.; Chen, W-H., (2017). Band selection in Sentinel-2 satellite for agriculture applications. Proceedings of the 23rd International Conference on Automation and Computing, University of Huddersfield, Huddersfield, UK.

Zhang, K.; Gann, D.; Ross, M.; Robertson, Q.; Sarmiento, J.; Santana, J.R.; Fritz, C., (2019). Accuracy assessment of ASTER, SRTM, ALOS, and TDX DEMs for Hispaniola and implications for mapping vulnerability to coastal flooding. Remote Sens. Environ., 225: 290-306 (**17 pages**).

**AUTHOR (S) BIOSKETCHES**

**Puno, G.R.,** Ph.D., Professor, Department of Forest Resources Management, College of Forestry and Environmental Science, Central Mindanao University, Musuan, Maramag, Philippines. Email: *grpuno@cmu.edu.ph*

**Puno, R.C.C.**, M.Sc., Instructor, Department of Environmental Science, College of Forestry and Environmental Science, Central Mindanao University, Musuan, Maramag, Philippines. Email: *rccpuno@cmu.edu.ph*

**Maghuyop, I.V.,** M.Sc., Instructor, Department of Environmental Science, College of Forestry and Environmental Science, Central Mindanao University, Musuan, Maramag, Philippines. Email: *ivmcfes@cmu.edu.ph*

**COPYRIGHTS**

©2021 The author(s). This is an open access article distributed under the terms of the Creative Commons Attribution (CC BY 4.0), which permits unrestricted use, distribution, and reproduction in any medium, as long as the original authors and source are cited. No permission is required from the authors or the publishers.

**HOW TO CITE THIS ARTICLE**

*Puno, G.R.; Puno, R.C.C.; Maghuyop, I.V., (2021). Two-dimensional flood model for risk exposure analysis of land use/land cover in a watershed. Global J. Environ. Sci. Manage., 7(2): 225-238.*

**DOI:** 10.22034/gjesm.2021.02.06

**url:** https://www.gjesm.net/article_239480.html